Supplemental Materials for Article

Unexpected diversity of ferredoxin-dependent thioredoxin reductases in cyanobacteria

Rubén M. Buey[1]*, David Fernández-Justel[1], Gloria González-Holgado[2], Marta Martínez-Júlvez[3], Adrián González-López[2], Adrián Velázquez-Campoy[3,4,5,6], Milagros Medina[3], Bob B. Buchanan[7], Monica Balsera[2*]

[1]Metabolic Engineering Group, Departamento de Microbiología y Genética, Universidad de Salamanca, Salamanca 37007, Spain

[2]Instituto de Recursos Naturales y Agrobiología de Salamanca (IRNASA-CSIC), Salamanca 37008, Spain

[3]Departamento de Bioquímica y Biología Molecular y Celular, Facultad de Ciencias, Instituto de Biocomputación y Física de Sistemas Complejos (GBsC-CSIC and BIFI-IQFR Joint Units), Universidad de Zaragoza, Zaragoza 50018, Spain

[4]Aragon Institute for Health Research (IIS-Aragon), Zaragoza 50009, Spain

[5]Biomedical Research Networking Center in Digestive and Hepatic Diseases (CIBERehd), Madrid 28029, Spain

[6]Fundación ARAID, Government of Aragon, Zaragoza, Spain

[7]Department of Plant & Microbial Biology, University of California, Berkeley CA 94708, USA

***Correspondence to:** monica.balsera@csic.es or ruben.martinez@usal.es

Supplemental Table S1. Data collection and refinement statistics.

	GvDTR-GvFdx1
Wavelength	0.9159
Resolution range	83.37-2.23 (2.47-2.23)
Space group	C 2 2 21
Unit cell	166.741 181.312 80.369 90 90 90
Total reflections	729970 (53087)
Unique reflections	59795 (2004)
Multiplicity	13.1 (10.2)
Completeness (ellipsoidal %)	93.7 (64.5)
Mean I/sigma(I)	9.3 (1.6)
Wilson B-factor	29.6
R-merge	0.30 (1.67)
R-meas	0.31 (1.76)
R-pim	0.085 (0.55)
CC1/2	0.989 (0.584)
Reflections used in refinement	40054
Reflections used for R-free	2035
R-work	0.201
R-free	0.232
Number of non-hydrogen atoms	6733
macromolecules	6169
ligands	308
solvent	256
Protein residues	855
RMS(bonds)	0.007

RMS(angles)	1.17
Ramachandran favored (%)	96.81
Ramachandran allowed (%)	3.19
Ramachandran outliers (%)	0.00
Rotamer outliers (%)	0.16
Clashscore	6.10
Average B-factor	37.21
macromolecules	36.55
ligands	54.57
solvent	32.07
Number of TLS groups	19
PDB code	6XTF

Statistics for the highest-resolution shell are shown in parentheses.

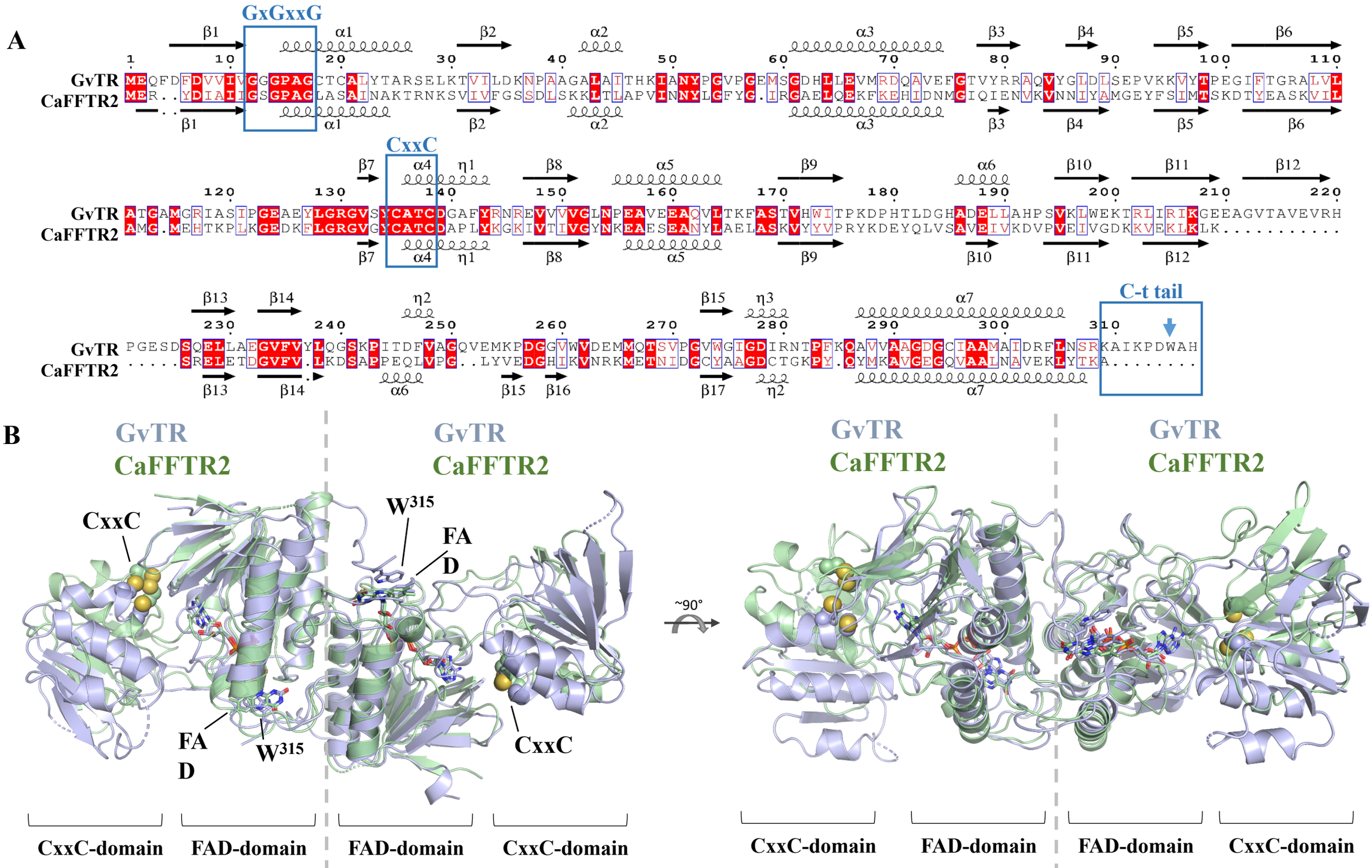

Supplemental Figure S1. Structural comparison of GvDTR with CaFFTR2. **(A)** Alignment of amino acid sequences between GvDTR and CaFFTR2 (mean % identity: 26.50, mean % similarity: 71.45). Functionally relevant segments, including amino acids directly implied on FAD binding (GxGxxG), the CxxC motif and the C-terminal tail in GvDTR with the conserved Trp residue, are boxed. Secondary structure elements, as revealed from the GvDTR and CaFFTR2 crystal structures, are indicated. The figure has been prepared with ESPrit (38); **(B)** Side and top view of the structural superposition between GvDTR (in green; PDB ID 5J60) and CaFFTR2 (in light orange; PDB ID 6GNA). The FAD cofactor and the side-chain of the Trp315 residue are depicted in sticks. The side-chain of the Cys amino acids in the redox-active disulfide domain (CxxC-domain in the figure) are shown in spacefill.

A

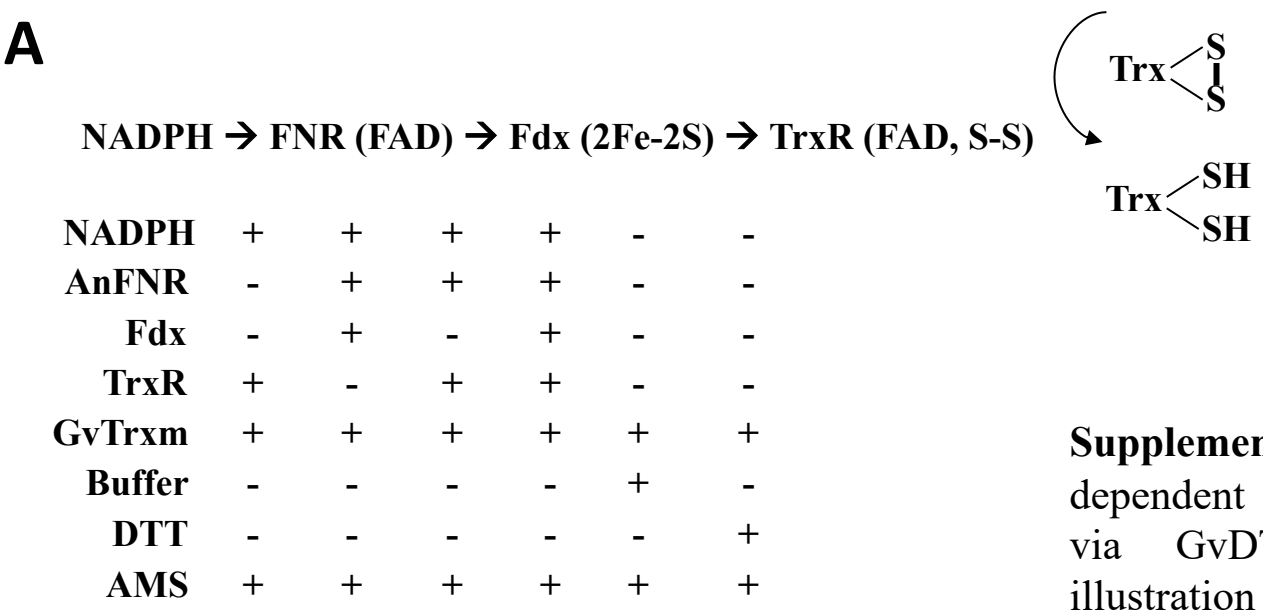

B

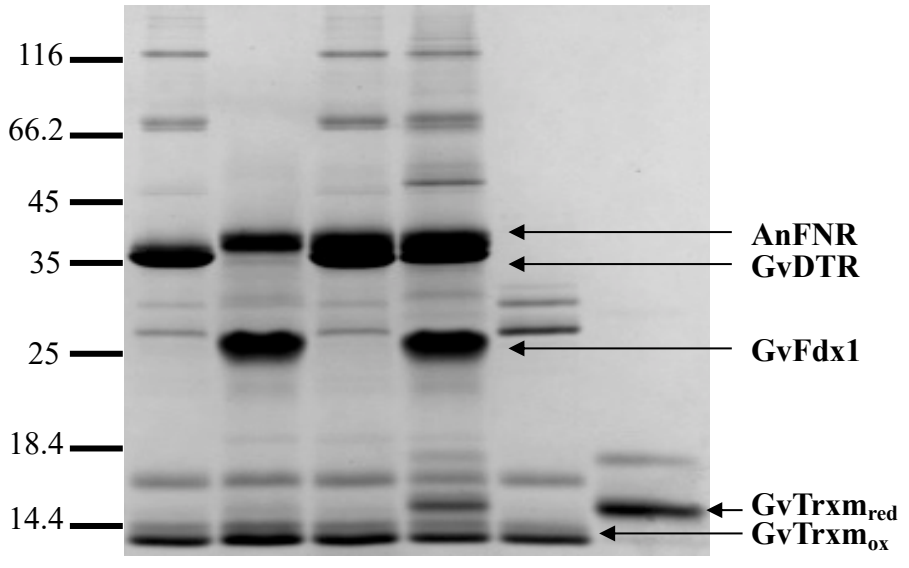

C

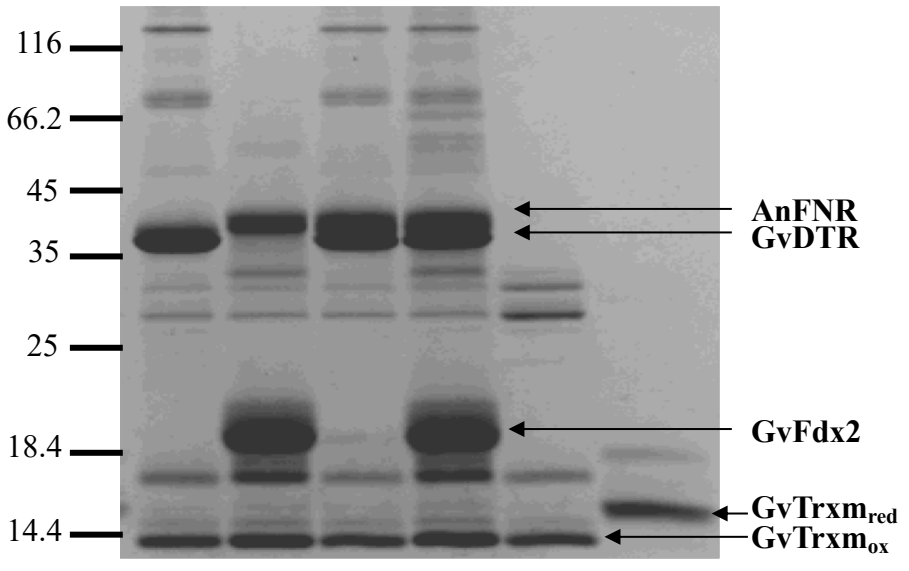

D

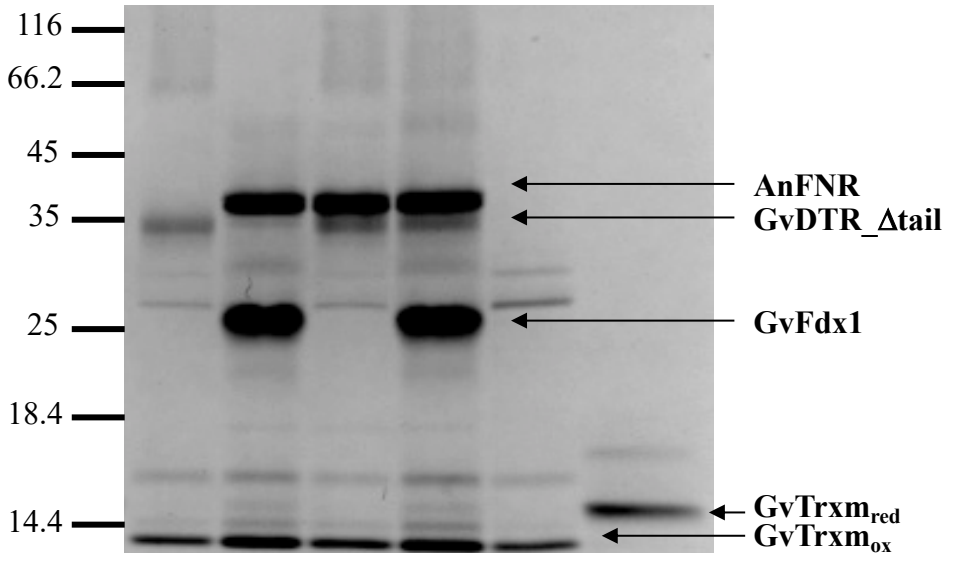

Supplemental Figure S2. Fdx-dependent reduction of GvTrx-m via GvDTR. **(A)** Schematic illustration of the *in vitro* reaction performed in this study for the reduction of Trx by DTR, with electrons derived from [2Fe-2S] Fdx, itself reduced by *Anabaena*´s FNR in the presence of NADPH. The reaction mixtures contained equal amounts of Trx, NADPH and some or all of the components included in the scheme depicted in **(A)**, as indicated for the reactions of GvDTR-WT with GvFdx1 **(B)**, GvDTR-WT with GvFdx2 **(C)** and GvDTR_Δtail with GvFdx1 **(D)**. After reaction, free sulfhydryl groups were labelled with AMS, which increases the mass of the protein by about 0.5 kDa per free thiol. The two different redox states of GvTrx-m (reduced or oxidized, $Trxm_{red}$ or $Trxm_{ox}$ respectively) were separated by SDS-PAGE under non-reducing conditions. GvTrx-m in the oxidized state (buffer) and in the reduced state (after incubation with DTT) are included for comparison. The position of the molecular weight markers (116, 66.2, 45, 35, 25, 18.4 and 14.4 kDa) are marked by bold lines to the left of the gels. The gels correspond to those shown in Figure 2 in the main text.

CP12	+	+	+	+	-	+	+
NADPH	+	+	+	+	+	-	-
AnFNR/GvFdx1	+	+	+	-	+	-	-
GvDTR	-	+	+	+	+	-	-
GvTrxm	-	-	+	+	+	-	-
DTT	-	-	-	-	-	-	+
AMS	+	+	+	+	+	+	+

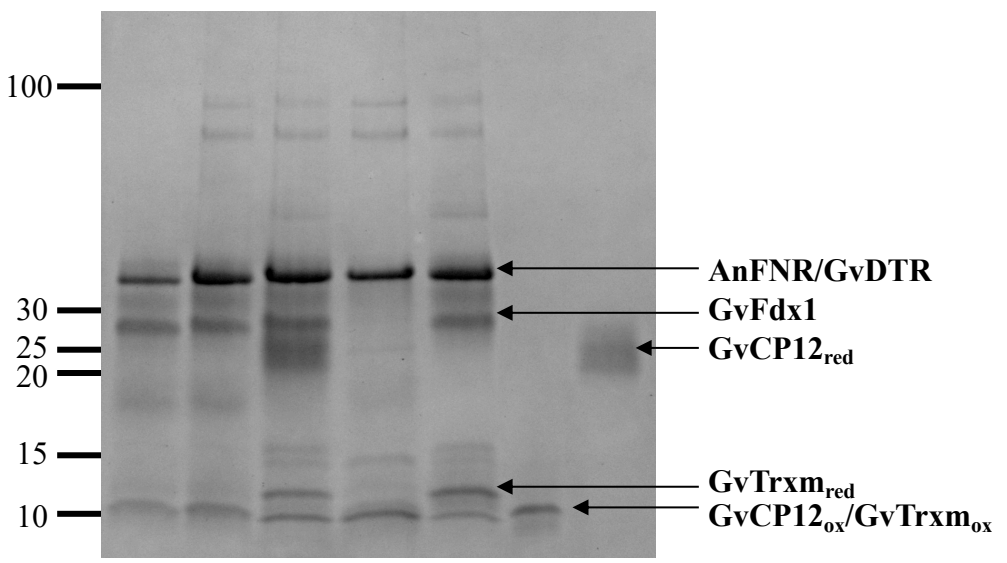

Supplemental Figure S3. Fdx-dependent reduction of GvCP12 via GvDTR. (A) Schematic illustration of the *in vitro* reaction performed in this study for the reduction of Trx, and further CP12, by DTR, as indicated in Figure S2; **(B)** The reaction mixtures contained equal amounts of Trx, NADPH and some or all of the components included in the scheme depicted in **(A)**. The experiment was performed as indicated in Figure S2. The reduced and oxidized states of GvCP12 ($GvCP12_{red}$ and $GvCP12_{ox}$) were separated by non-reducing SDS-PAGE after AMS treatment in the presence or absence of the components included in the complete scheme shown in **(A)**. GvCP12 in the oxidized state (buffer) and in the reduced state (after DTT incubation) are included for comparison. The position of the molecular weight markers (100, 30, 25, 20, 15 and 10 kDa) are marked by bold lines on the left of the gels. The gel corresponds to that shown in Figure 2 in the main text.

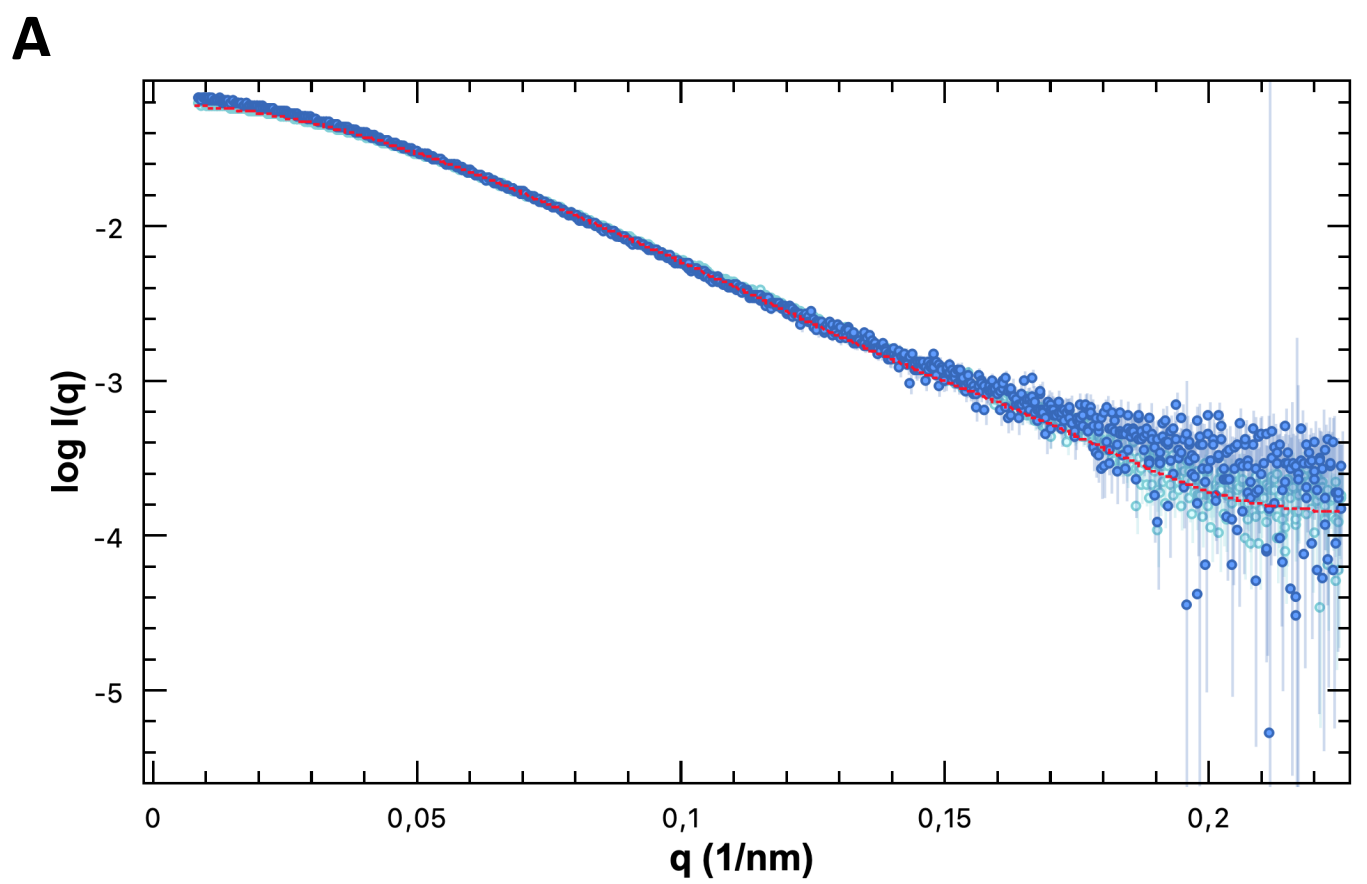

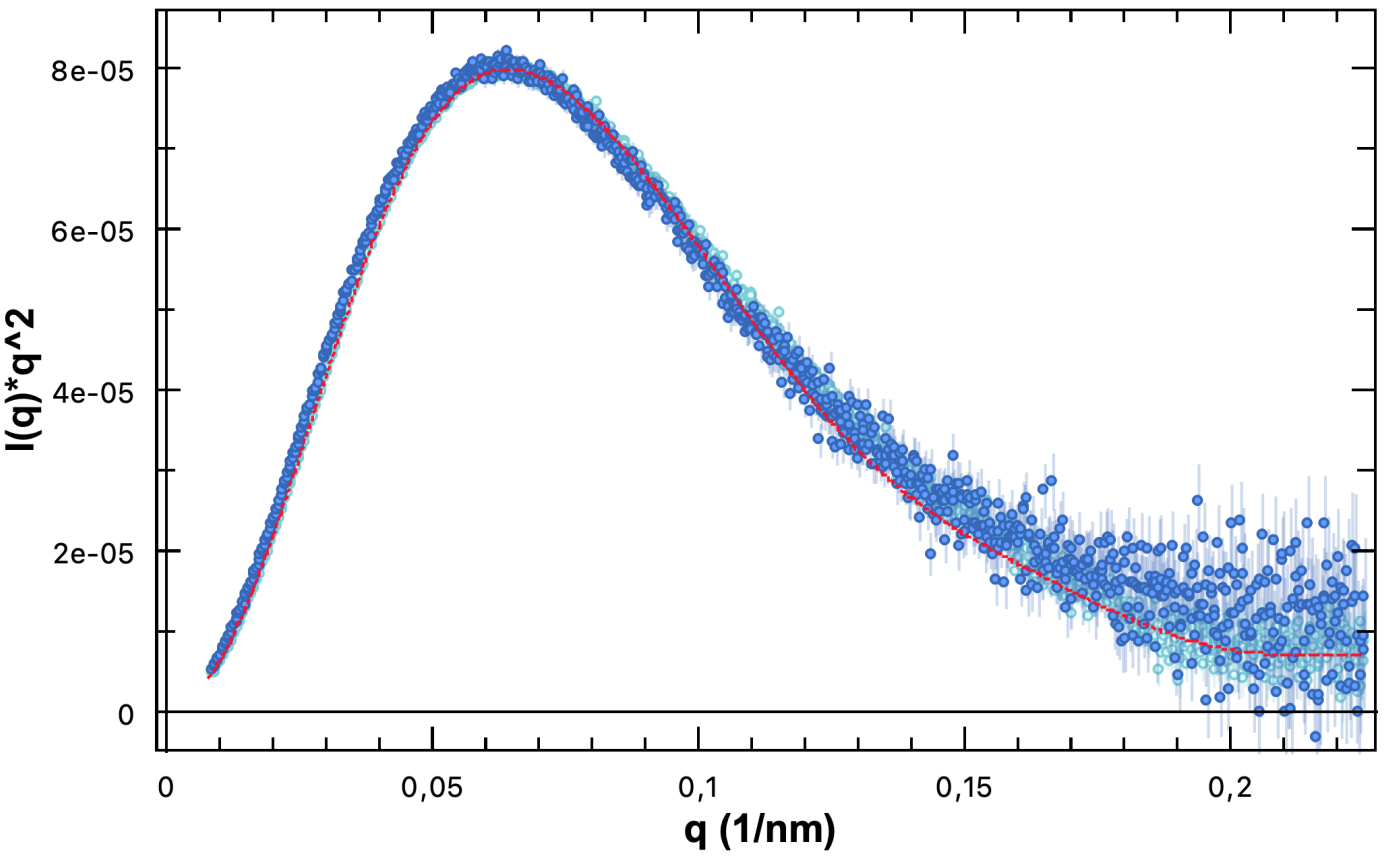

Supplemental Figure S4. SAXS analysis of GvDTR and GvDTR_Δtail. Experimental SAXS intensity **(A)** and Kratky **(B)** profiles of GvDTR (light blue), fitted to the theoretical profile of the crystallographic structure PDB code 5J60 (dashed red line), and GvDTR_Δtail (dark blue). Kratky profiles for both wild type and Δtail enzymes showed bell-shaped curves with a well-defined maximum, indicative of globular folded proteins, in concordance to their size exclusion chromatograms. The estimated radii of gyration are 3.0 and 3.2 nm for wild type and Δtail proteins, respectively, suggesting that removal of the C-terminal tail slightly "relaxes" the conformation of the dimer.

A

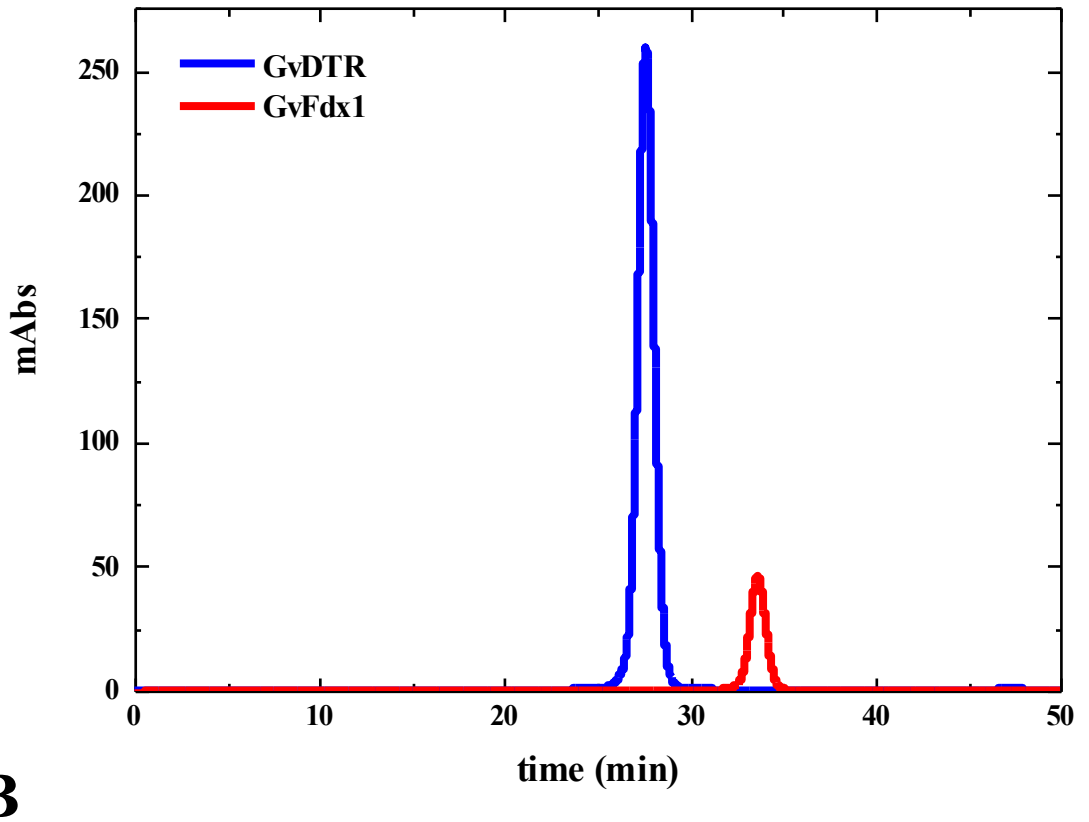

B

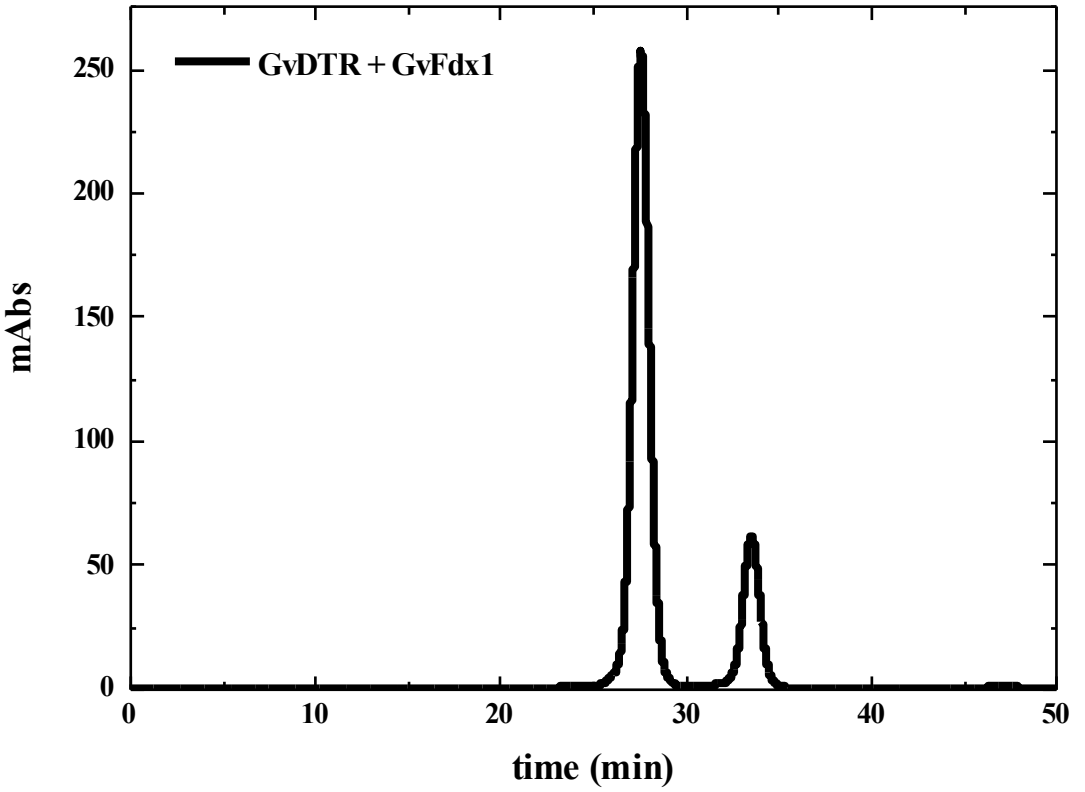

Supplemental Figure S5. GvDTR-GvFdx1 interaction analysis monitored by analytical gel filtration. **(A)** Superposition of the individual elution profiles of GvDTR (blue) and GvFdx1 (red). **(B)** Elution profile of a mixture of GvDTR and GvFdx1, after one hour incubation at room temperature.

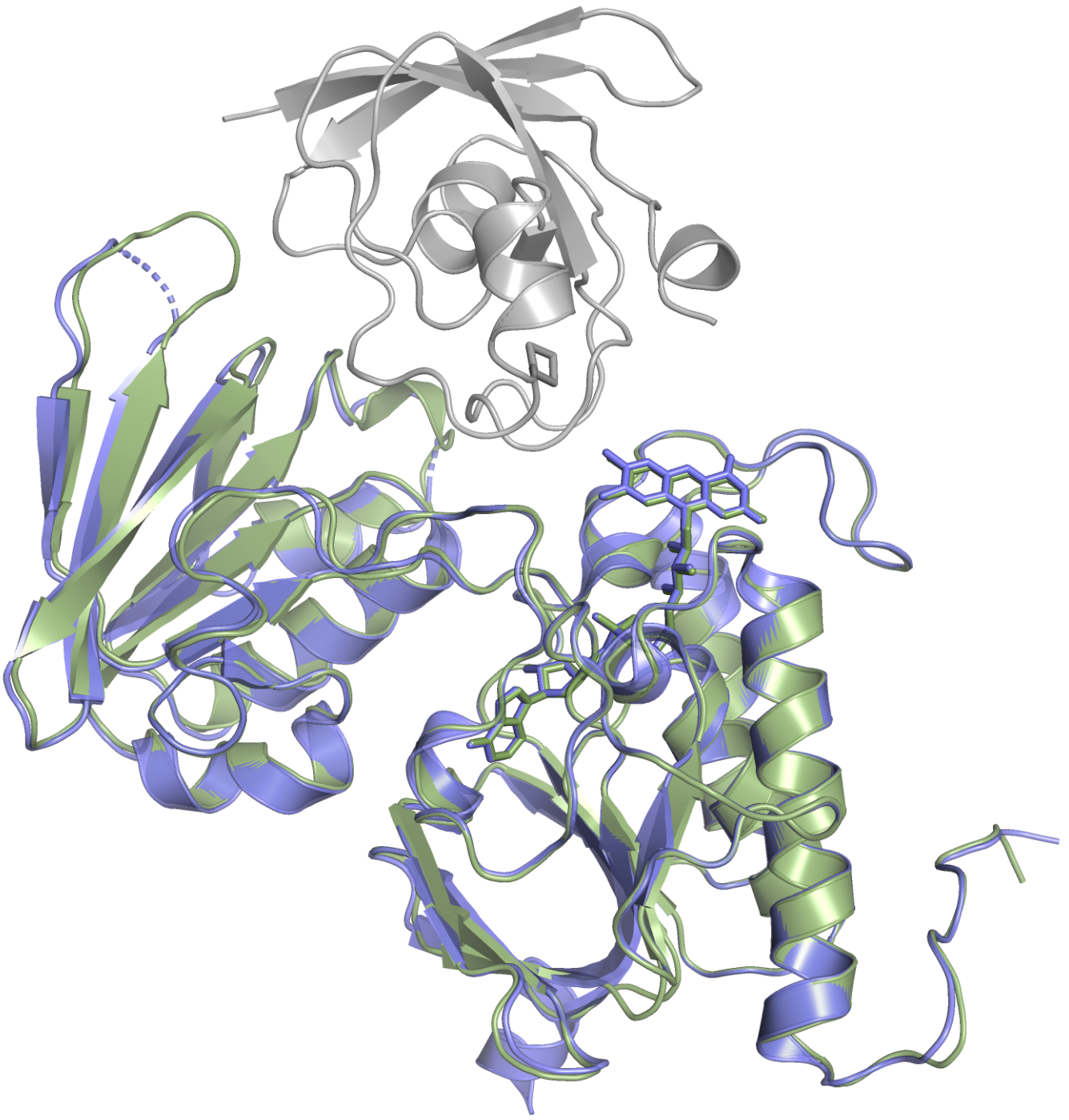

Supplemental Figure S6. Conformation of GvDTR in the presence and absence of Fdx. Structural alignment of a monomer of GvDTR in the presence (green; this work) or absence (blue, PDB code 5J60) of Fdx (grey; this work). Fe-S cluster and FAD cofactors are shown in sticks.

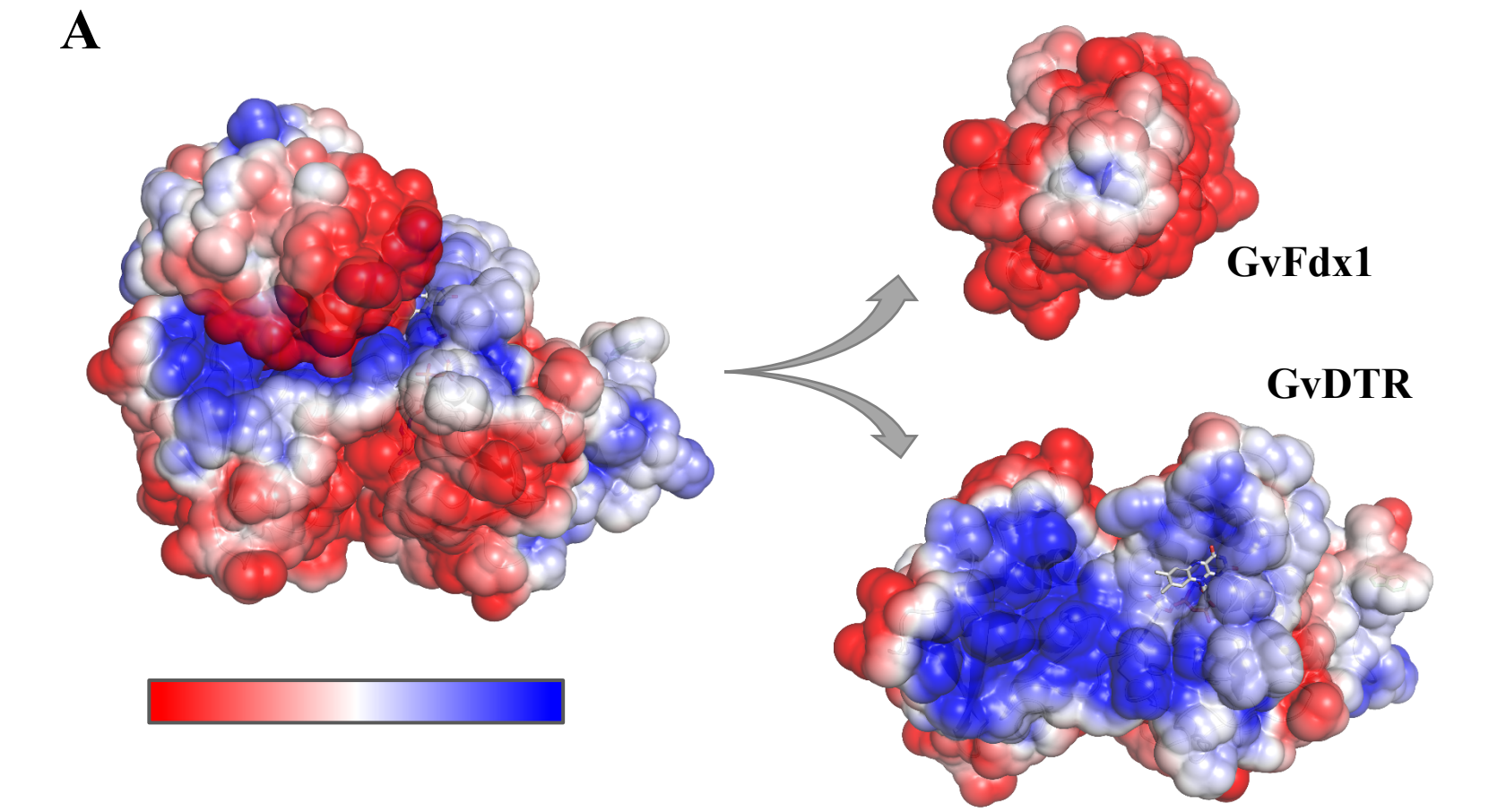

Supplemental Figure S7. Interaction of GvDTR with GvFdx. **(A)** Color-coded representation of the electrostatic potential at the solvent accessible surface of the complex GvDTR -Fdx1. The calculation was performed with APBS and represented with PyMOL. Color oscillates from -2.0 (red) to +2.0 (blue) K_bT/e_c.; **(B)** The most relevant residues involved in the interaction Fdx-FTR are shown in sticks. In GvDTR most of these residues are located in loops of the redox-active disulfide domain of a monomer (Lys177/Asp27, Lys200/Asp22, Arg202/Asp58 and Asp61, His220/Asp22), or are provided by the C-terminal tail of the adyacent monomer (Arg308/Asp94, Lys309/Asp68, Lys312/Asp94).